Oxide-Based RRAM: Uniformity Improvement Using A New Material-Oriented Methodology

B. Gao, H.W. Zhang, S. Yu, B. Sun, L.F. Liu, X.Y. Liu, Y. Wang, R.Q. Han, J.F. Kang*, B. Yu†, Y.Y. Wang
Institute of Microelectronics, Peking University, Beijing 100871, China, *E-mail: kangjf@pku.edu.cn
†College of Nanoscale Science and Engineering, State University of New York, Albany, NY 12203, USA

Abstract

For the first time, a new technical solution is presented to essentially improve the uniformity of oxide based RRAM devices by using material design methodology based on first principle calculations. The results indicate that doping of trivalent elements such as Al, La, or Ga into the tetravalent metal oxides such as HfO_2 or ZrO_2 effectively controls the formation of oxygen vacancy filaments along the doping sites, which helps improving the resistive switching (RS) behaviors in oxide based RRAM devices. The improved uniformity of forming and set/reset behaviors in the Al-doped HfO_2 RRAM devices was demonstrated by both experiments and theoretical calculations, proving the validity of the proposed method.

Keyword: RRAM, uniformity, resistive switching.

Introduction

Resistive random access memory (RRAM) has emerged as one of the most promising candidates for future "universal memory" [1-3]. Seeking effective way to reduce the fluctuations of key resistive switching (RS) parameters between the two resistance states [4] remains a critical challenge. It has been widely accepted that the formation and rupture of conducting oxygen vacancy (V_o) filaments (CF) are responsible for the switching between high resistance state (HRS) and low resistance state (LRS) [5]. In this paper, a new methodology to essentially improve the uniformity of RS behaviors in oxide-based RRAM devices is demonstrated for the first time. The first principle calculations suggest that trivalent La- or Al-doped HfO_2 or ZrO_2 are the most promising material combinations for RRAM application. TiN/HfO_2/Pt and TiN/Al-doped HfO_2/Pt devices were fabricated. The improved uniformity of key memory parameters in the Al-doped HfO_2 devices was demonstrated with better cross-wafer variation, verifying the validity of the proposed solution.

First Principle Calculations

The density functional theory (DFT) calculations were carried out by using a generalized gradient approximation (GGA) for the exchange-correlation potential and Vanderbilt-type ultrasoft pseudopotentials as implemented in the CASTEP code [6] to evaluate the forming energy of oxygen vacancy (E_f^O). E_f^O is defined as $E_f^O = E_{vac} - E_{free} + E_{O2}/2$, where E_{vac}, E_{free}, and E_{O2} represent the total energies of the vacancy and vacancy-free system, and the energy of the O_2 molecule, respectively. To calculate the first two parameters, a supercell with 96 atoms was constructed, as shown in Fig.1. The energy of the vacancy system is calculated by removing one oxygen atom from the supercell. The doping system is calculated by replacing one host atom with a doping atom. The impacts of the doping elements with different valences and ionic radii on E_f^O were addressed. The calculated values of E_f^O of the selected materials are summarized in Table I. From the Table, the trivalent elements such as Al, La, or Ga doping in the host materials with high E_f^O such as HfO_2 or ZrO_2 causes the lower E_f^O, which implies that V_o can be easily formed near the doping' sites. However, low value of E_f^O may cause retention issues of HRS [7]. The Al- or La-doped HfO_2 or ZrO_2 is found to be the most promising material systems for the RRAM application.

Experiments

To verify the proposed method, undoped and Al-doped HfO_2 based RRAM devices were fabricated. Pure Hf layer of 20nm or Al/Hf/Al sandwiched layer (5/20/5 nm) was deposited on Pt/Ti/SiO_2/Si substrates by DC sputtering, respectively. After two-step furnace annealing process at 600°C (10min in N_2 ambient and then 20min in O_2 ambient), the TiN top electrodes were deposited by reactive sputtering. The HfO_2 and Al-doped HfO_2 coated samples were patterned by traditional optical lithography to form isolated square-shape memory cells. The cross-sectional TEM image and the corresponding EDX profile of the Al-doped device are shown in Fig.2, indicating that Al atoms are diffused through the complete HfO_2 layer.

Results and Discussion

The statistical distributions of key memory parameters were measured. Fig.3 shows the DC behaviors of the undoped and Al-doped HfO_2 devices. The significantly reduced forming voltage was observed in Al-doped devices as compared with that in undoped devices, supporting the assumption that Al-doping causes the lower E_f^O. Fig.4 compares the forming voltage distributions of Al-doped devices with undoped devices. The wide dispersion in the undoped devices could be attributed to random CFs formed in the RS layers during each forming process, as shown in Fig. 5(a). Oppositely, narrow distribution of forming voltages was observed in Al-doped devices, which could be attributed to the fixed CFs steadily formed along the Al-doping sites, as illustrated in Fig.5 (b). If the stable CFs were generated along the Al-doping sites during the forming process, uniform set/reset behaviors would be also expected. Fig. 6 shows the set voltage distribution by dc sweep mode for the undoped and Al-doped devices. The predicted improvement in the uniformity was demonstrated in Al-doped devices.

Figs.7-8 compare the statistical distributions of HRS resistance (R_{LRS}) and LRS resistance (R_{HRS}) from cycle to cycle between the undoped and Al-doped devices. Significantly reduced dispersions of both R_{LRS} and R_{HRS} are observed in the Al-doped devices. These indicate that cycle-to-cycle uniformity is improved by Al doping into HfO_2. Fig.9 shows the forming voltage dispersion as a function of device area in the Al-doped HfO_2 device. Only negligible dependency was observed.

Furthermore, a numerical simulation program was developed to investigate the forming process based on the Monte Carlo method [8]. The schematic flow chart of the simulator is shown in Fig.10. The simulated Q_{BD} distribution under different doping concentration is shown in Fig.11, where Q_{BD} represents the critical amount of V_O when forming process occurs. The large slopes in the doping case imply the narrow distribution of the forming voltages. This is highly consistent with the measured results as shown in Fig.4. Fig.12 presents that the simulated Q_{BD} distributions are independent on the device area and layer thickness, similar to the measured results as shown in Fig.9. This suggests that the uniformity improvement in doped devices can be sustained with device scaling.

Conclusion

Based on the first principle calculations, a new technical solution to significantly improve the uniformity of key device parameters in oxide-based RRAM is demonstrated for the first time. The results indicate that fundamental improvements of the RS behavior in oxide-based RRAM devices can be achieved by using optimized material systems, providing important guidelines for the design and optimization of future-generation oxide-based RRAM technology.

Acknowledgement

The authors would like to thank Mr H.B. Dai at SMIC and the staff of the State Key Laboratory of Micro/Nano Fabrication Technology in Peking University for their help in the samples fabrication. This work is partially supported by 973 & 863 Programs (2006CB3027002& 2008AA031401).

Reference

[1]H. Y. Lee et al. IEDM Tech. Dig. 2008, p297; [2]C. Ho et al. Symp. on VLSI Technol.2007, p228; [3]N. Xu et al. Symp. on VLSI Technol.2008, p100;. [4]G. I. Meijer, Science, **319**, p1625 (2008); [5]R. Waser et al., Nature Materials, **6**, p834 (2007); [6] M. D. Segall et al, J. Phys: Condens. Matter, **14**, p2717 (2002); [7]B. Gao et al., IEDM Tech. Dig. 2008, p563; [8]R. Degraeve et al., TED, 45, p904 (1998).

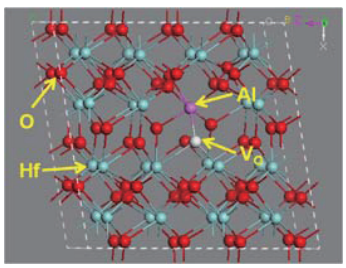

Fig.1 Schematic view of 96 atoms in HfO_2 supercell with one oxygen vacancy and one Al doping atom.

Table I Summary of the calculated E_f^O in selected materials

	Undoped (eV)	Ti (eV)	Al (eV)	La (eV)	Ga (eV)
HfO_2	6.53/6.40[a]	6.48	4.09	3.42	–
ZrO_2	6.37/5.09[b]	6.11	3.66	3.74	3.77
ZnO	4.79/5.05[c]	–	–	–	–

[a]A. S. Foster et al. Phys. Rev. B **65**, 174117(2002)
[b]A. S. Foster et al. Phys. Rev. B **64**, 224108(2001)
[c]T. R. Paudel et al. Phys. Rev. B **77**, 205202(2008)

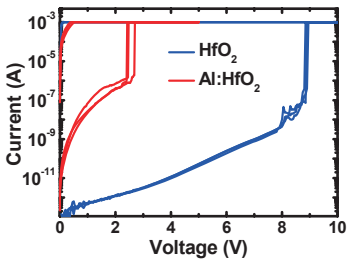

Fig.3 I-V curves of forming process. Lower forming voltage is measured in Al-doped HfO_2 devices.

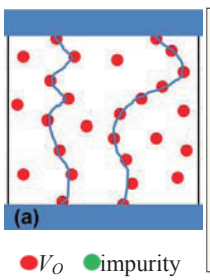

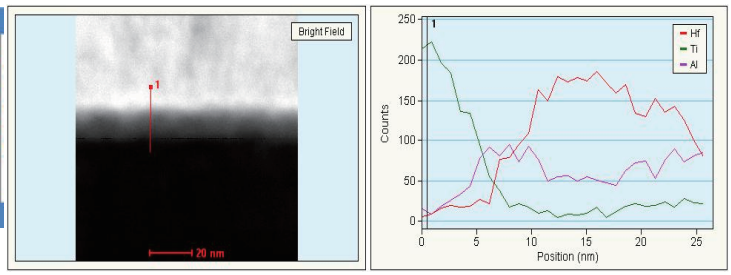

Fig.2 Cross-sectional TEM image (Left) and corresponding EDX profile (Right) of the TiN/Al-doped HfO_2/Pt device. The Al signal in HfO_2 layer indicates that Al atoms were doped into HfO_2 bulk.

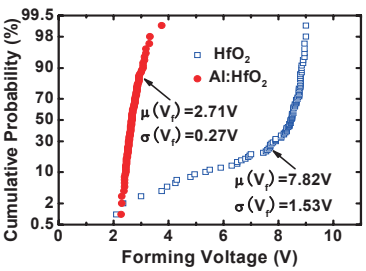

Fig.4 Distribution of the forming voltage for HfO_2 and Al-doped HfO_2 devices. The uniformity of the forming voltage is significantly improved by Al doping in HfO_2.

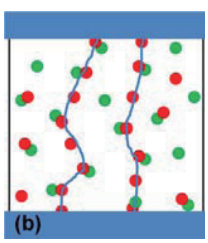

Fig.5 Schematic views to illustrate the formation of CF after forming process for: (a) undoped device and (b) doped device. The CF in undoped device forms randomly.

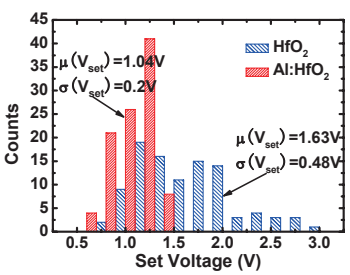

Fig.6 Set voltage distribution of HfO_2 and Al-doped HfO_2 devices under dc sweeping mode. Better uniformity is achieved in Al-doped HfO_2.devices.

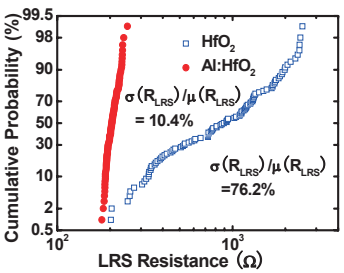

Fig.7 Distribution of R_{LRS} for HfO_2 and Al-doped HfO_2 under pulse voltage switching, where **μ/σ** represents the ratio of standard error over the average value.

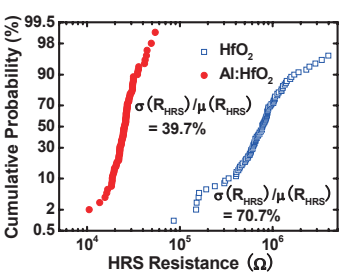

Fig.8 Distribution of R_{HRS} in HfO_2 and Al-doped HfO_2 devices. The Al-HfO_2 sample shows better uniformity but less R_{HRS}/R_{LRS} ratio than HfO_2 sample.

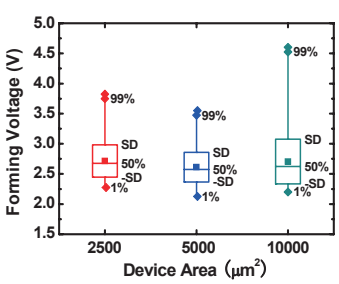

Fig.9 Forming voltage distribution as a function of device area for Al-doped HfO_2. The dispersion is only weekly dependant on device area.

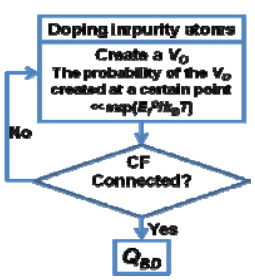

Fig.10 Schematic flow chart of the developed simulator based on the Monte Carlo type method.

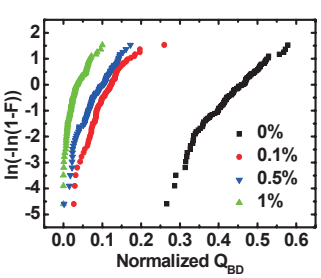

Fig.11 Simulated normalized Q_{BD} distribution as a function of doping concentration. The increased Weibull slopes are shown with doping concentrations.

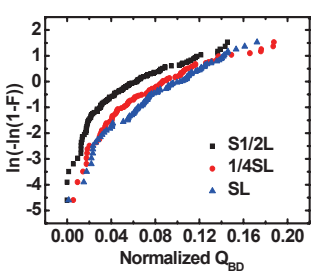

Fig.12 Simulated normalized Q_{BD} distribution as a function of device area or layer thickness. S and t in the figure refer to area and thickness, respectively.